Title: BATF relieves hepatic steatosis by inhibiting PD1 and promoting energy metabolism

Authors: Zhiwang Zhang[#1,3], Qichao Liao[#1], Tingli Pan[1], Lin Yu[1], Zupeng Luo[1], Songtao Su[1], Shi Liu[1], Menglong Hou[1], Yixing Li[2], Turtushikh Damba[4], Yunxiao Liang[1], Lei Zhou*[1]

Author affiliations: 1. Guangxi Academy of Medical Sciences, the People's Hospital of Guangxi Zhuang Autonomous Region, Nanning, China; 2. College of Animal Science and Technology, Guangxi University, Nanning, China; 3. Hebei Medical University, Shijiazhuang, China; 4. School of Pharmacy, Mongolian National University of Medical Sciences, Ulan Bator, Mongolia.

***Corresponding author:** Prof. Lei Zhou, E-mail: zhoulei@gxu.edu.cn; Guangxi Academy of Medical Sciences, the People's Hospital of Guangxi Zhuang Autonomous Region, Nanning, 530021, China. Prof. Guo Zhang, E-mail: zhangguogx@hotmail.com; Guangxi Academy of Medical Sciences, the People's Hospital of Guangxi Zhuang Autonomous Region, Nanning, 530021, China.

Data available on request from the authors:

The data that support the findings of this study are available from the corresponding author upon reasonable request. Some data may not be made available because of privacy or ethical restrictions.

Conflict of interest disclosure:

We state that no data reported in this manuscript has been published elsewhere or is under consideration for publication elsewhere. We state there is no conflict of interest.

Author contribution statement:

The study was conceived and planned by Zhiwang Zhang, Qichao Liao and Lei Zhou. Tingli Pan, Lin Yu, Zupeng Luo, Songtao Su, Shi Liu, Menglong Hou, Yixing Li, Turtushikh Damba, Yunxiao Liang helped with the experiment. The manuscript was written by Zhiwang Zhang and Lei Zhou. # means contributed equally. All other authors approved the manuscript prior to submission. All authors have seen the manuscript and approved to submit to your journal.

Acknowledgements

This work was supported by National Natural Science Foundation of China (32272952); Guangxi Science Foundation for Distinguished Young Scholars (2020GXNSFFA297008); Guangxi Natural Science Foundation (2019GXNSFDA245029).

Summary

The rising prevalence of nonalcoholic fatty liver disease (NAFLD) has become a global health threat that needs to be addressed urgently. Basic leucine zipper ATF-like transcription factor (BATF) is commonly thought to be involved in immunity, but its effect on lipid metabolism is not clear. Here, we investigated the function of BATF in hepatic lipid metabolism. BATF alleviated high-fat diet (HFD)-induced hepatic steatosis and inhibited elevated programmed cell death protein (PD)1 expression induced by HFD. A mechanistic study confirmed that BATF regulated fat accumulation by inhibiting PD1 expression and promoting energy metabolism. PD1 antibodies alleviated hepatic lipid deposition. In conclusion, we identified the regulatory role of BATF in hepatic lipid metabolism and that PD1 is a target for alleviation of NAFLD. This study provides new insights into the relationship between BATF, PD1 and NAFLD.

Introduction

Nonalcoholic fatty liver disease (NAFLD) has become a prevalent chronic liver disease that threatens human health globally. Studies have shown that the global prevalence of NAFLD is about 25% and this trend is still rising[1]. The clinical

52 diagnostic criterion for NAFLD is that >5% of the liver has steatosis[2]. Further
53 deterioration of NAFLD leads to nonalcoholic steatohepatitis (NASH)[3] and liver
54 fibrosis, markedly increased risk of adverse outcomes including overall mortality, and
55 liver-specific morbidity and mortality, respectively[4].

56 Transcription factors (TFs) are a class of DNA-binding proteins whose gene
57 regulation ability is critical to the molecular state of cells[5]. Multiple studies have
58 shown that TFs are closely related to NAFLD. The currently discovered TFs related to
59 liver lipid metabolism include peroxisome proliferator-activated receptors (PPARs)[6],
60 liver X receptors (LXRs)[7] and sterol-regulatory element binding proteins (SREBPs)[8].
61 These TFs are essential for maintaining the body's lipid metabolism balance through
62 the regulation of lipid metabolism genes[9]. Drugs targeting TFs have been developed,
63 and are widely used in the prevention and treatment of lipid metabolic disorders such
64 as obesity, hyperlipidemia, diabetes, etc., and show excellent clinical effects and
65 potential applications[10-11].

66 Basic leucine zipper ATF-like transcription factor (BATF), BATF2 and BATF3
67 belong to the activator protein (AP)-1 family[12]. Initially, BATF family members were
68 only considered to be inhibitors of AP-1-driven transcription, but recent studies have
69 found that these TFs have unique transcriptional activities in dendritic cells, B cells
70 and T cells[13]. This indicates that their functions may not be fully understood.
71 Currently, BATF has not been found to be directly related to lipid metabolism. The
72 purpose of this study was to explore this relationship. Our study provides a new
73 perspective for understanding the occurrence of NAFLD.

Results

BATF reduces high-fat-diet-induced lipid accumulation in hepatocytes

High-fat diet (HFD) promotes hepatic lipid accumulation and leads to dysregulation of lipid metabolism. We detected hepatic BATF expression in mice fed an HFD for 14 weeks to investigate the role of BATF in hepatic lipid metabolism. HFD significantly increased liver lipid deposition and BATF levels in mice (Fig 1A, B). HepG2 cells were treated with oleic acid/palmitic acid (OA/PA) to mimic HFD. It promoted triglyceride (TG) accumulation (Fig S1A) and increased BATF expression (Fig 1C). Our analysis of data from patients with NAFLD showed that BATF levels increased with increasing NAFLD score (Fig 1D). We inhibited BATF in HepG2 cells (Fig S1B) and found no effect on cellular TG accumulation (Fig 1E). This indicated that inhibition of BATF could not regulate lipid deposition in hepatocytes (Fig 1F). Therefore, the role of BATF overexpression was studied. Oil red O staining on lipid droplets and TG detection showed that BATF alleviated OA/PA-induced HepG2 cellular fat deposition (Fig 1G, H). BATF also reduced TG accumulation in L02 human hepatocytes (Fig 1I, J). To confirm the results, we isolated mouse primary hepatocytes and infected them with a virus expressing BATF. The results also showed that BATF alleviated accumulation of lipid droplets and TG (Fig 1K, L). In AML12 cells, we found consistent results (Fig S1C, D). These results confirm that BATF can alleviate lipid deposition in hepatocytes.

95 **Increased hepatic BATF alleviates HFD-induced hepatic steatosis in mice**

96 We constructed an AAV8 virus overexpressing BATF to infect mouse liver. After
97 infection, mice were fed normal chow or HFD. The weight and fat mass of the mice
98 were measured weekly, and the mice were sacrificed 12 weeks after virus infection
99 (Fig 2A). Overexpression of BATF increased hepatic BATF protein expression (Fig
100 2B), but there was no change in heart, muscle, fat or spleen (Fig 2C). In addition,
101 HFD increased body weight and adiposity in mice, while BATF significantly
102 alleviated weight gain and fat accumulation (Fig 2D, E). Mouse livers showed that
103 HFD made them yellow and covered with fat-like particles, but BATF significantly
104 alleviated these changes (Fig 2F). Liver hematoxylin and eosin (HE) staining of mice
105 in the HFD group confirmed that BATF reduced the number of unstained vacuoles
106 (lipid droplets) (Fig 2G). To verify the effect of BATF on hepatic lipid metabolism, oil
107 red O staining and TG content were examined and confirmed that BATF significantly
108 alleviated HFD-induced lipid deposition (Fig 2H–J). BATF had no effect on the liver
109 total cholesterol (TC) content of mice (Fig 2K). BATF did not have a significant
110 impact on glucose metabolism in mice, including blood glucose levels (Fig S2A),
111 Glucose Oxidase activity (Fig S2B) and glucose tolerance (Fig S2C, D).

112 We conducted further studies to explore the mechanism by which BATF regulated
113 hepatic lipid metabolism. BATF reduced alanine aminotransferase (ALT) and
114 aspartate aminotransferase (AST) activities (Fig 3A, B). It confirmed that BATF
115 alleviated HFD-induced liver injury in mice. Detection of mRNA expression of lipid
116 metabolism genes revealed that BATF did not affect lipid-synthesis-related genes (Fig

117 3C), but promoted expression of various lipid hydrolysis genes, including *Ampk, Aco*,
118 *Acox1*, *Bcl2*, *Cpt1*, etc (Fig 3D). Fatty acid β-oxidation is a main route of fat
119 metabolism, in which short-chain acyl coenzyme A dehydrogenase (SCAD) plays a
120 key role. The result confirmed that BATF greatly promotes SCAD activity (Fig 3E).
121 Fatty acid oxidation mainly takes place in mitochondria, so studies on the effect of
122 BATF on aerobic oxidation were carried out. BATF elevated the level of ATP (Fig
123 3F). An oxygen consumption rate test was performed to explore the effect of BATF on
124 mitochondrial oxygen consumption rate (Fig 3G), and indicated that BATF increased
125 basal respiration, maximal respiration and ATP production in HepG2 cells (Fig 3H).
126 These results suggest that BATF mitigates the effects of HFD on hepatic lipid
127 deposition by promoting energy metabolism.

128 **BATF alleviates HFD-induced adipocyte hypertrophy in mice**

129 BATF alleviated HFD-induced increase in adiposity (Fig 2D). After anesthetizing the
130 mice, we used micro-computed tomography (CT) to scan the whole body and image
131 the adipose tissue (Fig 4A). The red lightly shaded parts represent the adipose tissue
132 of the mice, and the results indicated that BATF alleviated overall fat accumulation.
133 The epididymal fat and subcutaneous fat of mice were separated. The results showed
134 that BATF reduced the epididymal and subcutaneous fat (Fig 4B–E). HE staining of
135 mouse adipose tissue allowed microscopic observation of adipocytes, and the
136 diameter and area of the adipocytes indicated that BATF alleviated adipocyte
137 hypertrophy (Fig 4F–K). BATF was overexpressed only in the liver but not in adipose

138 tissue. To investigate the effect of BATF on lipid accumulation in adipocytes, we
139 overexpressed BATF in 3T3-L1 cells and found that it had no effect on accumulation
140 of TG (Fig 4L). These results confirm that BATF does not directly act upon
141 adipocytes to reduce fat accumulation. Therefore, we speculated that BATF regulates
142 fat accumulation in adipose tissue by influencing secretion of substances from the
143 liver. To test this conjecture, we cultured differentiated 3T3-L1 cells with HepG2-
144 cultured cell culture medium (overexpressing BATF) and assayed their TG content.
145 The HepG2-cultured cell culture medium (overexpressing BATF) alleviated TG
146 accumulation in 3T3-L1 cells (Fig 4M). Interleukin (IL)-27 has an inhibitory effect on
147 fat accumulation. We confirmed that HFD decreased IL-27 expression, while BATF
148 enhanced IL-27 expression (Fig 4N). This suggests that BATF mitigates the expansion
149 of adipose tissue by promoting IL-27 secretion.

150 **BATF alleviates hepatocyte lipid accumulation by inhibiting programmed cell**
151 **death protein 1**

152 Several studies have confirmed that there is a regulatory relationship between BATF
153 and programmed cell death protein (PD)1[14-16]. HFD increased PD1, while BATF
154 inhibited PD1 expression in mouse liver (Fig 5A). These results were confirmed in
155 HepG2 cells (Fig 5B). To determine the role of PD1 in lipid accumulation in
156 hepatocytes, we overexpressed PD1 in HepG2 cells and assayed the lipid content.
157 Both oil red O staining and TG content confirmed that PD1 promoted lipid deposition
158 in hepatocytes (Fig 5C, D). PD1 antibody inhibited the role of PD1 and successfully

159 alleviated TG accumulation in hepatocytes, but BATF overexpression plus PD1
160 antibody did not further alleviate lipid deposition (Fig 5E), suggesting that BATF
161 regulates lipid deposition through PD1. To confirm this hypothesis, we overexpressed
162 BATF and PD1. Overexpression of BATF decreased TG, while the TG-lowering
163 effect of BATF disappeared when PD1 was overexpressed (Fig 5F). To determine the
164 regulatory role of BATF on PD1, we constructed a luciferase vector containing 2000
165 bp upstream of the transcription start site of PD1. BATF decreased the transcriptional
166 activity of PD1 promoter, confirming the role of BATF in regulating PD1 expression
167 (Fig 5G). These results suggest that BATF regulates lipid deposition through
168 inhibition of PD1. In conclusion, HFD leads to an increase in the level of PD1
169 transcription in the liver. BATF promotes lipolysis and energy consumption in
170 hepatocytes by regulating PD1 transcription, thereby reducing HFD-induced liver
171 lipid deposition and alleviating NAFLD (Fig 5H).

172 **PD1 antibody alleviates HFD-induced obesity and liver steatosis in mice**

173 PD1 plays an important role in tumorigenesis as a tumor immune escape target, and
174 PD1 antibodies as antitumor drugs can inhibit PD1 and mitigate tumor growth and
175 cancer development[17]. Our study confirmed that PD1 promoted lipid deposition in
176 hepatocytes (Fig 5C, D), and *in vivo* experiments were performed to verify the role of
177 PD1 on hepatic steatosis in mice fed an HFD. PD1 antibody alleviated HFD-induced
178 weight gain in mice after intraperitoneal injection of PD1 antibody (200 μg) (Fig 6A).
179 The mice injected with PD1 antibody were smaller than the control mice (Fig 6B).

180 The results of fat mass confirmed that PD1 antibody alleviated fat accumulation in
181 mice (Fig 6C). The epididymal and subcutaneous fat of mice were reduced by PD1
182 antibody (Fig 6D–G). Mouse livers showed that HFD gave them an appearance of
183 hepatic steatosis, which was significantly alleviated by PD1 antibody (Fig 6H). The
184 liver was stained with Oil Red O and assayed for TG content, which showed that PD1
185 antibody reduced accumulation of lipid droplets (Fig 6I) in the liver and alleviated
186 lipid deposition (Fig 6J). We extracted RNA from mouse livers and examined
187 expression of lipolysis-related genes. PD1 antibody treatment was consistent with
188 overexpression of BATF, and both promoted expression of lipolysis-related genes (Fig
189 6K). Similarly, PD1 antibody treatment promoted SCAD activity in mouse liver,
190 suggesting fatty acid β-oxidation was enhanced (Fig 6L).

191 **Discussion**

192 In the present study, we found that HFD elevated BATF expression in mouse liver.
193 We also found that inhibition of hepatocyte BATF did not regulate lipid deposition,
194 while overexpression of BATF decreased TG accumulation. Studies on hepatocytes
195 confirmed that BATF regulated hepatocyte lipid deposition. BATF also alleviated
196 HFD-induced obesity in mice, not by directly acting on adipose tissue but by
197 influencing IL-27, which acts as a regulator of fat deposition[18]. The regulation of
198 hepatic lipid metabolism by BATF has not previously been investigated. Here, we
199 found that BATF mitigated HFD-induced increase in PD1 expression. We revealed
200 that PD1 promoted hepatocyte lipid deposition. Through luciferase assays, we found

201 that BATF regulated lipid deposition by inhibiting PD1 expression. Experiments in
202 mice confirmed that PD1 inhibition alleviated HFD-induced obesity and hepatic
203 steatosis.

204 The adaptive immune system has evolved to eliminate virtually any threat from
205 the organism[19]. PD1 is expressed during T-cell activation and through T-cell receptor
206 counteracting positive signaling by engaging its ligands PDL1 and/or PDL2[20]. PD1
207 regulates the immune system and promotes self-tolerance by downregulating the
208 immune response to human cells and by suppressing T-cell inflammatory activity[21].
209 The development of checkpoint blockade inhibitors has revolutionized cancer
210 immunotherapy[22] and has led to durable survival outcomes in some patients with
211 metastatic disease[23]. Previous studies on PD1 have focused on the immune system,
212 and we found that HFD increased its expression in the liver of mice (Fig 5A). This is
213 consistent with previous studies[24] suggesting that PD1 is equally important in the
214 liver. Several studies have demonstrated that PD1 and BATF regulate each other to
215 modulate immune system flexibility[25-26]. We hypothesized that BATF and PD1 co-
216 regulate the hepatic immune system to affect lipid deposition. Our results confirm our
217 conjecture that BATF reduces fat accumulation by inhibiting PD1, confirming that
218 PD1 is downstream of the BATF signaling pathway (Fig 5F, G).

219 Cancer and autoimmune disease are closely related, and many therapeutic
220 antibodies are widely used in clinics for the treatment of both diseases. Moreover,
221 immune checkpoint blockade using the anti-PD1/PD-L1/CTLA4 antibody has been
222 shown to improve prognosis of patients with refractory solid tumors[27]. In this study,

223 we used PD1 antibodies to treat HFD-induced obesity and NAFLD in mice.
224 Surprisingly, PD1 antibody has an excellent therapeutic effect on obesity and
225 NAFLD. PD1 antibodies reduced adiposity and hepatic lipid deposition (Fig 6), which
226 is consistent with overexpression of BATF. There have been no approved drugs for
227 NAFLD treatment. In this study, the effect of PD1 antibodies on NAFLD treatment
228 was encouraging. Our findings have somewhat pioneered the cognition of BATF, PD1
229 and its expansion with NAFLD therapy.

230 **Materials and methods**

231 **Animals**

232 All animal studies were approved by the Animal Ethics Committee of Guangxi
233 University (GXU-2020-288). Four-week-old male C57BL/6J mice were purchased
234 from Guangxi Medical University (Nanning, China) and kept in individual cages on a
235 12-h light/dark cycle with free access to water and food at room temperature. At week
236 10, mice were injected intravenously (tail vein) with 200 μl adeno-associated virus
237 (AAV). AAV was HBAAV2/8-CMV-m-BATF-3×flag-ZsGreen and HBAAV/8-
238 ZsGreen (packaged by HANBIO, Shanghai, China). The mice were fed with a normal
239 diet (ND) (AIN93) or HFD (D12492) for 12 weeks[28]. To study the effect of PD1
240 inhibitors on NALFD, the mice were fed with HFD and rat IgG (ab37361; Abcam) or
241 anti-mouse PD1 (AB10949053, Bio X Cell) antibody was administered
242 (intraperitoneal injection) at 200 μg/mouse twice weekly[29]. Body weight and fat mass
243 were recorded weekly, and body composition (fat) was determined by Body

244 Composition Analyzer (QMR-23-060H-I; Suzhou, China). Mice were anesthetized
245 with 2.4% tribromoethanol (T48402, Sigma–Aldrich) to evaluate fat content, and
246 micro-CT images were taken using a micro-CT scanner (SKYSCAN1278; Bruker,
247 Belgium). All groups were randomized and blinded to form equal-sized groups of at
248 least three (exact numbers are given in the legend).

249 **Human disease data**

250 The human data of NAFLD were taken from the Gene Expression Omnibus,
251 Accession Number GSE130970[30].

252 **Cell culture and transfection**

253 HepG2 (HB-8065, ATCC), L02 (YUCHI Biology, China), Hepa1-6 (CRL-1830,
254 ATCC), HEK293T (ACS-4500, ATCC), 3T3L1 (CL-173, ATCC) cells were cultured
255 in DMEM medium (C11995500BT, Gibco) supplemented with fetal bovine serum
256 (04-400-1A, BI) and 1% penicillin–streptomycin (P1400, Solarbio, China). The
257 AML12 cell (CRL-2254, ATCC) culture medium was DMEM/F12 (Gibco) containing
258 10% FBS and 1% penicillin–streptomycin. The cells were incubated at 37°C and 5%
259 carbon dioxide. For simulating HFD *in vitro*, 200 μM OA and 100 μM PA were
260 conjugated to bovine serum albumin (BSA) as previously described[31].

261 For transfection of plasmids or siRNA oligos, Hieff Trans Liposomal Transfection
262 Reagent (40802ES02, YEASEN) was used. Plasmid constructs were created using the
263 eukaryotic expression vector pcDNA3.1-[32]. Mice BATF (NM_016767.2), PD1
264 (NM_008798.3) CDS were cloned from mouse liver cDNA. RNAi sequence was
265 synthesized from Sangon Biotech (Shanghai, China).

266 **Primary hepatocyte isolation and AAV infection**

267 The abdominal cavity of 8-week-old male mice was opened after anesthesia with
268 2.4% tribromoethanol. The inferior vena cava was cannulated with a 23G needle and
269 perfused with 30 mL perfusion buffer (1×HBSS without Ca^{2+}, Mg^{2+} supplemented
270 with 0.5 mM EDTA and 25 nM HEPES). The liver was digested by 25 mL of 37℃
271 digestion buffer (1×HBSS with Ca^{2+}, Mg^{2+} supplemented with 1 μg/mL collagenase
272 type II and 1M HEPES). Following the perfusion, the liver was gently removed and
273 massaged through 70 μm nylon mesh with 10 mL of 4℃ precooled complete medium
274 (DMEM supplemented with 1% FBS). Hepatocytes were isolated by centrifugation at
275 50 *g*, 4°C, for 2 min. After discarding the supernatant, hepatocytes were resuspended
276 in 10 mL complete medium containing 5 mL freshly prepared 90% Percoll solution (9
277 mL Percoll with 1 mL PBS). Cell debris was removed by centrifugation at 200 *g*, 4°C,
278 for 10 min. The supernatant was aspirated, resuspended and centrifuged at 50 *g*, 4℃
279 for 2 min, after resuspension in William E medium supplemented 1% glutamine and
280 1% penicillin–streptomycin. Cell resuspension was transferred into a 0.1% gelatin-
281 coated plate and incubated at 37°C, 5% carbon dioxide[33]. Cells were maintained for
282 24 h in medium. For *in vitro* experiments with AAV, 1 μL f purified HBAAV2/8-
283 CMV-m-BATF-3×flag-ZsGreen or HBAAV/8-ZsGreen was added to cultured
284 hepatocytes to achieve high BATF overexpression.

285 **Glucose tolerance test**

286 Glucose tolerance test (GTT) was performed as previously described[34]. Mice were
287 fasted for 16 h and injected with D-glucose at 2 g/kg intraperitoneally. The blood

288 glucose level was measured at 0,15, 30, 60 and 120 min after glucose injection.

289 **Western blotting**

290 Tissues were lysed with 1 mL RIPA lysis buffer and supplemented 1% protease
291 inhibitor cocktail (Solarbio) for 2–5 min with steel balls in a tissue lyser (Qiagen,
292 Germany). Tissue lysates were incubated with the buffer at 4°C overnight (cell
293 samples were incubated in lysis buffer for 30 min at 4°C). The lysate was centrifuged
294 at 12,000 rpm for 10 min, the supernatant was collected, and the protein concentration
295 was determined using the BCA method (P0011, Beyotime Biotechnology). The
296 supernatant was mixed with loading buffer and boiled at 100°C for 10 min. Samples
297 were loaded and subjected to 10% SDS-PAGE. After transfer to PVDF membranes,
298 blots were blocked with 5% skimmed milk powder and incubated with primary
299 antibody overnight at 4°C. The primary antibodies included a BATF antibody (8638S,
300 Cell Signaling Technology, USA), anti-β-actin (GB11001, Servicebio, China), and β-
301 tublin (15115, Cell Signaling Technology). Secondary antibody was goat anti-rabbit
302 (Jackson, 111-035-003), images were acquired using the BIO-RAD protein gel
303 imaging system (Universal hood II), and band intensity was calculated using Image
304 J[35].

305 **TGs, TC and glycerin detection**

306 Cells or tissues were prepared according to the instructions of the A110-1-1
307 Triglyceride Assay Kit[36], A111-1-1 Total Cholesterol Assay Kit (Nanjing Jiancheng
308 Bioengineering Institute, China), and Tissue Cell Glycerin Test kit (E1024, Pulilai,
309 China). Liver tissues or cells were lysed by RIPA lysis buffer. Samples were

310 centrifuged at 12 000 rpm for 10 min, and the supernatants were collected.
311 Supernatants (10 μL) were added to a 96-well plate and 190 μL working solution was
312 added to each well. The plate was incubated at 37°C for 10 min. The microplate
313 reader (Tecan M200 PRO) recorded the contents of TG, TC and glycerin, then
314 normalized using the protein concentration.

315 **Enzyme activity assay**

316 SCAD enzyme activity in cultured cells or liver tissues was detected using the SCAD
317 Assay Kit (Gen Med, Plymouth, MN, USA). The liver tissue activities of ALT and
318 AST were measured using the C009-2-1 ALT Reagent Kit and C010-2-1 AST
319 Reagent Kit (Nanjing Jiancheng Bioengineering Institute, China).

320 **ATP measurements**

321 Cellular ATP content was measured using a luciferin/luciferase-based kit (S0026,
322 Beyotime Biotechnology, China).

323 **HE and Oil Red O staining**

324 HE and Oil Red O staining was performed as previously described[37]. Livers,
325 epididymal fat and subcutaneous fat of mice were dissected and fixed in 4%
326 paraformaldehyde overnight at 4°C. Samples were sent to Wuhan Service Technology
327 Co. Ltd. (Wuhan, China) for paraffin embedding, sectioning, and staining. Images
328 were collected by light microscope and Image J was used to examine the cell diameter
329 and the area.

330 **Oxygen consumption rate**

331 Oxygen consumption rate was measured by extracellular flux (XF24) analyzer
332 (Seahorse Bioscience). Cells were seeded at 2×10^4 per well in XF24 plates. The
333 probe plate was hydrated with the calibration solution (pH 7.4) and a 2 mM glutamine
334 assay solution (pH 7.35 ± 0.05) was prepared, and incubated for 16–20 h at 37°C and
335 5% CO_2. Culture medium was replaced by 2% FBS medium and incubated without
336 CO_2 for 1 h before the completion of probe cartridge calibration. Basal oxygen
337 consumption rate was measured after injection of oligomycin (1 μM), carbonyl
338 cyanide p-trifluoro-methoxyphenyl hydrazone (FCCP 1 μM), and rotenone/antimycin
339 A (ROT/AA) (0.5 μM)[38].

340 **RNA extraction and real-time quantitative polymerase chain reaction**

341 Total RNA was extracted by TRIzol Reagent (Life Technologies, USA). Reverse
342 transcription of RNA was performed with the Reverse Transcription System (A3500,
343 Promega), and formed cDNA from 1 μg total RNA. 2× RealStar Green Fast Mixture
344 was used for real-time quantitative polymerase chain reaction (PCR) (GenStar,
345 Beijing, China). The relevant primer sequences (5′-3′) were as follows: Human β-
346 actin forward: CACCATTGGCAATGAGCGGTTC, reverse:
347 AGGTCTTTGCGGATGTCCACGT. Human BATF forward:
348 GATGTGAGAAGAGTTCAGAGGAG, reverse:
349 GTTTCTCCAGGTCTTCGCTCTC. Mouse BATF forward:
350 ATGCCTCACAGCTCCGACAGC, reverse: TCAGGGCTGGAAGCGTGGC. Mouse
351 PD-1 forward: CGGTTTCAAGGCATGGTCATTGG, reverse:
352 TCAGAGTGTCGTCCTTGCTTCC; Mouse *Fasn* forward:

353 CACAGTGCTCAAAGGACATGCC, reverse: CACCAGGTGTAGTGCCTTCCTC.
354 Mouse *Srebp1* forward: CGACTACATCCGCTTCTTGCAG, reverse:
355 CCTCCATAGACACATCTGTGCC. Mouse *Gpam* forward:
356 GCAAGCACTGTTACCAGCGATC, reverse: TGCAATCAGCCTTCGTCGGAAG.
357 Mouse *Acc1* forward: GTTCTGTTGGACAACGCCTTCAC, reverse:
358 GGAGTCACAGAAGCAGCCCATT. Mouse Aco forward:
359 TCACAGCAGTGGGATTCCAA, reverse: TCTGCAGCATCATAACAGTGTTCTC.
360 Mouse *AcoxI* forward: TAACTTCCTCACTCGAAGCCA, reverse:
361 AGTTCCATGACCCATCTCTGTC. Mouse *Bcl2* forward:
362 ACTTCCACTACAGGACAGAC, reverse: TCTAAGGTGACTCGATATGG. Mouse
363 *Cpt1* forward: GCACTGCAGCTCGCACATTACAA, reverse:
364 CGTTGACATCCGTAAAGACC. Mouse *β-actin* forward:
365 AACAGTCCGCCTAGAAGCAC, reverse:
366 CTCAGACAGTACCTCCTTCAGGAAA. Mouse *Hsl* forward:
367 GGAGCACTACAAACGCAACGA, reverse: TCGGCCACCGGTAAAGAG. Mouse
368 Acc2 forward: AGAAGCGAGCACTGCAAGGTTG, reverse:
369 GGAAGATGGACTCCACCTGGTT. Mouse Atgl forward:
370 GGAACCAAAGGACCTGATGACC, reverse: ACATCAGGCAGCCACTCCAACA.

371 **Retroviral transduction**

372 Retroviral vectors pMSCV-PIG and pMSCV-PIG-BATF were used to infect 3T3L1
373 cells. The pMSCV-PIG-BATF viral vector was constructed, and the coding sequence
374 of mouse BATF was amplified from liver cDNA by PCR and cloned into the *Eco*RI

375 site using ClonExpress II One Step Cloning Kit (C112-01/02, Vazyme, China). To
376 obtain pseudotyped virus with the ability to infect, pMSCV-PIG-BATF, pMSCV-PIG-
377 GFP, and retroviral packaging plasmids (pKat and pCMV-VSV-G) were cotransfected
378 into subconfluent HEK293T cells. The virus stocks were collected 2 and 3 days after
379 transfection, centrifuged at 5000 *g* for 10 min, subpackaged and frozen at −80°C.
380 3T3L1 cells with around 30% confluence were treated with virus stock containing 8
381 μg/mL polybrene for 4 h, washed, and cultured in fresh medium.

382 **Luciferase assay for promoter activity analysis**

383 Firefly luciferase constructs were cloned using the pGL3-Basic vector as a backbone.
384 Target 5′ UTRs (PD1 was amplified by primers, forward:
385 AGCATGAGCCCTGAGGATTG reverse: CAGTGTCGCCTTCAGTAGCA) were
386 cloned upstream of Firefly luciferase in the pgl3. Renilla luciferase reporter vector
387 pRL-TK was gifted by State Key Laboratory for Conservation and Utilization of
388 Subtropical Agro-Bioresources. Hepa1-6 cells were inoculated into medium in 24-
389 well culture plates and cultured overnight. Cell transfection and cotransfection were
390 conducted when the cell density reached 80%. Dual Luciferase Reporter Assay was
391 performed 48 h post-transfection using the Dual-Lumi II Luciferase Reporter gene
392 Assay kit (PG089S). Renilla luciferase was used to normalize transfection efficiency
393 and luciferase activity.

394 **Statistical analysis**

395 All experiments were repeated at least in triplicate, and statistical analysis was done
396 using independent values. All data are presented as mean ± SD. Statistical analysis

397 was performed using Student's unpaired two-tailed *t* test (for two groups) or analysis
398 of variance (ANOVA) (for multiple groups). One-way ANOVA with Tukey's test was
399 conducted for comparisons. The differences were considered significant at $P < 0.05$
400 (*). Values with different letters were significantly different.

401 Reference

402 1. Younossi, Z. M.; Koenig, A. B.; Abdelatif, D.; Fazel, Y.; Henry, L.; Wymer, M., Global
403 epidemiology of nonalcoholic fatty liver disease-Meta-analytic assessment of prevalence, incidence,
404 and outcomes. *Hepatology* **2016,** *64* (1), 73-84.
405 2. Siddiqui, M. S.; Harrison, S. A.; Abdelmalek, M. F.; Anstee, Q. M.; Bedossa, P.; Castera, L.;
406 Dimick-Santos, L.; Friedman, S. L.; Greene, K.; Kleiner, D. E.; Megnien, S.; Neuschwander-Tetri, B.
407 A.; Ratziu, V.; Schabel, E.; Miller, V.; Sanyal, A. J.; Liver Forum Case Definitions Working, G., Case
408 definitions for inclusion and analysis of endpoints in clinical trials for nonalcoholic steatohepatitis
409 through the lens of regulatory science. *Hepatology* **2018,** *67* (5), 2001-2012.
410 3. Pierantonelli, I.; Svegliati-Baroni, G., Nonalcoholic Fatty Liver Disease: Basic Pathogenetic
411 Mechanisms in the Progression From NAFLD to NASH. *Transplantation* **2019,** *103* (1), e1-e13.
412 4. Cotter, T. G.; Rinella, M., Nonalcoholic Fatty Liver Disease 2020: The State of the Disease.
413 *Gastroenterology* **2020,** *158* (7), 1851-1864.
414 5. Simicevic, J.; Deplancke, B., Transcription factor proteomics-Tools, applications, and challenges.
415 *Proteomics* **2017,** *17* (3-4).
416 6. Gross, B.; Pawlak, M.; Lefebvre, P.; Staels, B., PPARs in obesity-induced T2DM, dyslipidaemia
417 and NAFLD. *Nat Rev Endocrinol* **2017,** *13* (1), 36-49.
418 7. Wang, Y.; Viscarra, J.; Kim, S. J.; Sul, H. S., Transcriptional regulation of hepatic lipogenesis. *Nat*
419 *Rev Mol Cell Biol* **2015,** *16* (11), 678-89.
420 8. Eberle, D.; Hegarty, B.; Bossard, P.; Ferre, P.; Foufelle, F., SREBP transcription factors: master
421 regulators of lipid homeostasis. *Biochimie* **2004,** *86* (11), 839-48.
422 9. Karagianni, P.; Talianidis, I., Transcription factor networks regulating hepatic fatty acid
423 metabolism. *Biochim Biophys Acta* **2015,** *1851* (1), 2-8.
424 10. Uyeda, K.; Repa, J. J., Carbohydrate response element binding protein, ChREBP, a transcription
425 factor coupling hepatic glucose utilization and lipid synthesis. *Cell Metab* **2006,** *4* (2), 107-10.
426 11. Mota de Sa, P.; Richard, A. J.; Hang, H.; Stephens, J. M., Transcriptional Regulation of
427 Adipogenesis. *Compr Physiol* **2017,** *7* (2), 635-674.
428 12. Sopel, N.; Graser, A.; Mousset, S.; Finotto, S., The transcription factor BATF modulates cytokine-
429 mediated responses in T cells. *Cytokine Growth Factor Rev* **2016,** *30:39-45.*
430 13. Murphy, T. L.; Tussiwand, R.; Murphy, K. M., Specificity through cooperation: BATF-IRF
431 interactions control immune-regulatory networks. *Nat Rev Immunol* **2013,** *13* (7), 499-509.
432 14. Wu, X.; Gu, Z.; Chen, Y.; Chen, B.; Chen, W.; Weng, L.; Liu, X., Application of PD-1 Blockade
433 in Cancer Immunotherapy. *Comput Struct Biotechnol J* **2019,** *23;17:661-674.* (2001-0370 (Print)).
434 15. Man, K.; Gabriel, S. S.; Liao, Y.; Gloury, R.; Preston, S.; Henstridge, D. C.; Pellegrini, M.; Zehn,

D.; Berberich-Siebelt, F.; Febbraio, M. A.; Shi, W.; Kallies, A., Transcription Factor IRF4 Promotes CD8(+) T Cell Exhaustion and Limits the Development of Memory-like T Cells during Chronic Infection. *Immunity* **2017,** *19;47(6):1129-1141* (1097-4180 (Electronic)).

16. Liu, Q.; Ou, Q.; Shen, L.; Qiu, C.; Zhang, B.; Zhang, W.; Shao, L.; Gao, Y.; Chen, Z. W., BATF Potentially Mediates Negative Regulation of PD-1/PD-Ls Pathway on T Cell Functions in Mycobacterium tuberculosis Infection. *Front Immunol* **2019,** *10*, 2430.

17. Ribas, A.; Wolchok, J. D., Cancer immunotherapy using checkpoint blockade. *Science* **2018,** *359* (6382), 1350-1355.

18. Wang, Q. A.-O.; Li, D.; Cao, G. A.-O.; Shi, Q.; Zhu, J.; Zhang, M.; Cheng, H.; Wen, Q.; Xu, H.; Zhu, L.; Zhang, H.; Perry, R. A.-O.; Spadaro, O.; Yang, Y. A.-O.; He, S.; Chen, Y.; Wang, B.; Li, G.; Liu, Z.; Yang, C.; Wu, X.; Zhou, L.; Zhou, Q.; Ju, Z. A.-O.; Lu, H.; Xin, Y.; Yang, X. A.-O.; Wang, C.; Liu, Y. A.-O.; Shulman, G. A.-O.; Dixit, V. D.; Lu, L. A.-O.; Yang, H. A.-O.; Flavell, R. A.-O.; Yin, Z. A.-O., IL-27 signalling promotes adipocyte thermogenesis and energy expenditure. *Nature* **2021,** *600(7888):314-318* (1476-4687 (Electronic)).

19. Sharpe, A. H.; Pauken, K. E., The diverse functions of the PD1 inhibitory pathway. *Nat Rev Immunol* **2018,** *18* (3), 153-167.

20. Freeman, G. J.; Long Aj Fau - Iwai, Y.; Iwai Y Fau - Bourque, K.; Bourque K Fau - Chernova, T.; Chernova T Fau - Nishimura, H.; Nishimura H Fau - Fitz, L. J.; Fitz Lj Fau - Malenkovich, N.; Malenkovich N Fau - Okazaki, T.; Okazaki T Fau - Byrne, M. C.; Byrne Mc Fau - Horton, H. F.; Horton Hf Fau - Fouser, L.; Fouser L Fau - Carter, L.; Carter L Fau - Ling, V.; Ling V Fau - Bowman, M. R.; Bowman Mr Fau - Carreno, B. M.; Carreno Bm Fau - Collins, M.; Collins M Fau - Wood, C. R.; Wood Cr Fau - Honjo, T.; Honjo, T., Engagement of the PD-1 immunoinhibitory receptor by a novel B7 family member leads to negative regulation of lymphocyte activation. *J Exp Med* **2000,** *2;192(7):1027-34* (0022-1007 (Print)).

21. Lei, Q.; Wang, D.; Sun, K.; Wang, L.; Zhang, Y., Resistance Mechanisms of Anti-PD1/PDL1 Therapy in Solid Tumors. *Front Cell Dev Biol* **2020,** *8*, 672.

22. Sharma, P.; Allison, J. P., The future of immune checkpoint therapy. *Science* **2015,** *3;348(6230):56-61*.

23. Pulendran, B. A.-O.; Davis, M. A.-O. X., The science and medicine of human immunology. *Science* **2020,** *25;369(6511):eaay4014*.

24. Wang, Z.; Aguilar, E. G.; Luna, J. I.; Dunai, C.; Khuat, L. T.; Le, C. T.; Mirsoian, A.; Minnar, C. M.; Stoffel, K. M.; Sturgill, I. R.; Grossenbacher, S. K.; Withers, S. S.; Rebhun, R. B.; Hartigan-O'Connor, D. J.; Mendez-Lagares, G.; Tarantal, A. F.; Isseroff, R. R.; Griffith, T. S.; Schalper, K. A.; Merleev, A.; Saha, A.; Maverakis, E.; Kelly, K.; Aljumaily, R.; Ibrahimi, S.; Mukherjee, S.; Machiorlatti, M.; Vesely, S. K.; Longo, D. L.; Blazar, B. R.; Canter, R. J.; Murphy, W. J.; Monjazeb, A. M., Paradoxical effects of obesity on T cell function during tumor progression and PD-1 checkpoint blockade. *Nat Med* **2019,** *25* (1), 141-151.

25. Quigley, M.; Pereyra, F.; Nilsson, B.; Porichis, F.; Fonseca, C.; Eichbaum, Q.; Julg, B.; Jesneck, J. L.; Brosnahan, K.; Imam, S.; Russell, K.; Toth, I.; Piechocka-Trocha, A.; Dolfi, D.; Angelosanto, J.; Crawford, A.; Shin, H.; Kwon, D. S.; Zupkosky, J.; Francisco, L.; Freeman, G. J.; Wherry, E. J.; Kaufmann, D. E.; Walker, B. D.; Ebert, B.; Haining, W. N., Transcriptional analysis of HIV-specific CD8+ T cells shows that PD-1 inhibits T cell function by upregulating BATF. *Nat Med* **2010,** *16* (10), 1147-51.

26. Ji, L. S.; Sun, X. H.; Zhang, X.; Zhou, Z. H.; Yu, Z.; Zhu, X. J.; Huang, L. Y.; Fang, M.; Gao, Y.

T.; Li, M.; Gao, Y. Q., Mechanism of Follicular Helper T Cell Differentiation Regulated by Transcription Factors. *J Immunol Res* **2020,** *2020*, 1826587.

27. Yasunaga, M., Antibody therapeutics and immunoregulation in cancer and autoimmune disease. *Semin Cancer Biol* **2020,** *64*, 1-12.

28. Qi, Y.; Zhang, Z.; Liu, S.; Aluo, Z.; Zhang, L.; Yu, L.; Li, Y.; Song, Z.; Zhou, L., Zinc Supplementation Alleviates Lipid and Glucose Metabolic Disorders Induced by a High-Fat Diet. *J Agric Food Chem* **2020,** *68* (18), 5189-5200.

29. Zelenay, S.; van der Veen, A. G.; Bottcher, J. P.; Snelgrove, K. J.; Rogers, N.; Acton, S. E.; Chakravarty, P.; Girotti, M. R.; Marais, R.; Quezada, S. A.; Sahai, E.; Reis e Sousa, C., Cyclooxygenase-Dependent Tumor Growth through Evasion of Immunity. *Cell* **2015,** *162* (6), 1257-70.

30. Hoang, S. A.; Oseini, A.; Feaver, R. E.; Cole, B. K.; Asgharpour, A.; Vincent, R.; Siddiqui, M.; Lawson, M. J.; Day, N. C.; Taylor, J. M.; Wamhoff, B. R.; Mirshahi, F.; Contos, M. J.; Idowu, M.; Sanyal, A. J., Gene Expression Predicts Histological Severity and Reveals Distinct Molecular Profiles of Nonalcoholic Fatty Liver Disease. *Sci Rep* **2019,** *9* (1), 12541.

31. Li, Q.; Li, Y.; Zhang, Z.; Kang, H.; Zhang, L.; Zhang, Y.; Zhou, L., SEIPIN overexpression in the liver may alleviate hepatic steatosis by influencing the intracellular calcium level. *Mol Cell Endocrinol* **2019,** *488*, 70-78.

32. Liang Huang, Q. L., Tingli Pan, Yu Sun, Zhier Aluo, Lianggui Xiao, Jingsu Yu, Siqi Liu, Yang Xiao, ; Yufeng Yang, Y. L., Lei Zhou, Small Intestine-specific Knockout of CIDEC Improves Obesity and Hepatic Steatosis by Inhibiting Synthesis of Phosphatidic Acid. *International Journal of Biological Sciences* **2022,** *18*, 5740.

33. Zhang, Z.; Liu, S.; Qi, Y.; Aluo, Z.; Zhang, L.; Yu, L.; Li, Q.; Luo, Z.; Sun, Z.; Zhou, L.; Li, Y., Calcium supplementation relieves high-fat diet-induced liver steatosis by reducing energy metabolism and promoting lipolysis. *J Nutr Biochem* **2021,** *94*, 108645.

34. Zhang, Z.; Luo, Z.; Yu, L.; Xiao, Y.; Liu, S.; Z, A. L.; Ma, Z.; Huang, L.; Xiao, L.; Jia, M.; Song, Z.; Zhang, H.; Li, Y.; Zhou, L., Ruthenium 360 and mitoxantrone inhibit mitochondrial calcium uniporter channel to prevent liver steatosis induced by high-fat diet. *Br J Pharmacol* **2022,** *179* (11), 2678-2696.

35. Zhang, Z.; Pan, T.; Sun, Y.; Liu, S.; Song, Z.; Zhang, H.; Li, Y.; Zhou, L., Dietary calcium supplementation promotes the accumulation of intramuscular fat. *J Anim Sci Biotechnol* **2021,** *12* (1), 94.

36. Zhang, Z.; Liao, Q.; Sun, Y.; Pan, T.; Liu, S.; Miao, W.; Li, Y.; Zhou, L.; Xu, G., Lipidomic and Transcriptomic Analysis of the Longissimus Muscle of Luchuan and Duroc Pigs. *Front Nutr* **2021,** *8*, 667622.

37. Luo, Z.; Hu, H.; Liu, S.; Zhang, Z.; Li, Y.; Zhou, L., Comprehensive analysis of the translatome reveals the relationship between the translational and transcriptional control in high fat diet-induced liver steatosis. *RNA Biol* **2021,** *18* (6), 863-874.

38. Liu, S.; Yang, D.; Yu, L.; Aluo, Z.; Zhang, Z.; Qi, Y.; Li, Y.; Song, Z.; Xu, G.; Zhou, L., Effects of lycopene on skeletal muscle-fiber type and high-fat diet-induced oxidative stress. *J Nutr Biochem* **2021,** *87*, 108523.

Figure legends

522 Figure 1. Effects of BATF on lipid deposition in hepatocytes under high-fat diet.
523 (A) The mice and liver Oil red O staining in normal diet group (CN) and high-fat diet
524 group (HFD). Bar, 1 cm (left panel) and 100 μm (right panel). (B) The protein
525 expression of BATF in liver tissues, (n = 4). (C) The mRNA expression of BATF in
526 liver tissues (n = 5). (D) Spearman correlation Analysis between TPM of BATF and
527 NAFLD Patients with Different Degrees, (n = 4-18). (E) Triglyceride content (n = 5).
528 (F) Detection of BATF overexpression in HepG2. (G) Oil red O staining of HepG2
529 cells with OA/PA when BATF was overexpressed and (H) triglyceride content, (n =
530 4). (I) Oil red O staining of L02 cells with OA/PA when BATF was overexpressed and
531 (J) triglyceride content, (n = 3). (K) Oil red O staining of primary hepatocytes with
532 OA/PA when BATF was overexpressed and (L) triglyceride content, (n = 3). The data
533 are expressed as mean ± SD. *P < 0.05 **P < 0.01.
534
535 Figure 2. Effects of BATF on hepatic fat deposition in mice.
536 (A) Experimental designs illustration of mice. (B) Expression of BATF protein in
537 liver, (n = 4). (C) Expression of BATF protein in various tissues of HFD-CN mice
538 (HBAAV/8-ZsGreen, WB in lane1, 3, 5, 7, 9) and HFD-BATF mice (HBAAV2/8-
539 CMV-m-BATF-3×flag-ZsGreen, WB in lane 2, 4, 6, 8, 10). (D) Mice bodyweight, (n
540 = 8-10). (E) Mice fat ratio, (n = 8-10). (F) Mice liver. Bar, 1 cm. (G) HE staining of
541 mice liver sections. Bar, 100 μm. (H) Oil red O staining of mice liver sections and
542 quantitative analysis. Bar, 100 μm, (n = 3). (J) Liver triglyceride levels, (n = 8-10).
543 (K) Liver total cholesterol (TC) levels, (n = 8-10).
544
545 Figure 3.
546 (A) ALT activity in mice liver, (n = 8). (B) AST activity in mice liver, (n = 7). (C) The
547 *Fasn*, *Srebp1*, *Gpam*, *Acc1* mRNA expression level in mice liver, (n = 6-8). (D) The
548 *Ampk*, *Aco*, *Acox1*, *Bcl2*, *Cpt1*, *Hsl*, *Acc2*, *Atgl* mRNA expression level in mice liver,
549 (n= 6-7). (E) SCAD activity in HepG2 cells with OA/PA treatment, (n = 4). (F) ATP
550 content in HepG2 cells with OA/PA treatment, (n = 4). (G) Oxygen consumption rate
551 (OCR). (H) Basal respiration, maximal respiration, proton leak and coupling
552 efficiency. The data are expressed as mean ± SD. *P < 0.05 **P < 0.01.
553
554 Figure 4.
555 (A) CT images of fat axial view. (B) eWAT of mice. Bar, 1 cm. (C) eWAT weight /
556 bodyweight, (n = 9-10). (D) iWAT of mice. Bar, 1 cm. (E) eWAT weight /
557 bodyweight, (n = 9-10). (F) HE staining of eWAT, (G) adipocyte diameter and (H) cell
558 area. Bar, 200 μm. (I) HE staining of iWAT, (J) adipocyte diameter and (K) cell area.
559 Bar, 200 μm. (L) Triglyceride content of undifferentiated 3T3L1 cells (n=5). (M)
560 Triglyceride content of differentiated 3T3L1 cells (n=3-4). (N) The mRNA expression
561 of IL27 in liver tissues (n = 5). The data are expressed as mean ± SD. *P < 0.05 **P <
562 0.01.
563
564 Figure 5. BATF alleviates hepatocyte lipid accumulation by inhibiting PD1.
565 (A) The mRNA expression of PD1 in liver tissues (n = 3). (B) The mRNA expression

566 of PD1 in HepG2 cells (n = 3). (C) Oil red O staining of HepG2 cells, Bar, 20 μm, (n
567 = 3). (D), (E), (F) Triglyceride content with OA/PA (n ≥ 3). (G) Dual luciferase assay
568 on Hepa1-6 cells cotransfected with firefly luciferase constructs containing the PD1
569 promoter, Renilla luciferase vector pRL-TK and pcDNA3.1(-) or pcDNA3.1(-)-BATF,
570 (n ≥ 3). (H) The Mechanism diagram of BATF alleviates hepatocyte lipid
571 accumulation by PD1. The data are expressed as mean ± SD. *P < 0.05 **P < 0.01.
572
573 Figure 6. Effects of PD1 antibody on liver lipid metabolism in HFD mice.
574 (A) Mice bodyweight, (n ≥ 5). (B) The mice were injected with IgG or PD1 antibody
575 under HFD, (n ≥ 5). (C) Mice fat ratio, (n ≥ 5). (D) eWAT of mice. Bar, 1 cm. (E)
576 eWAT weight / bodyweight, (n ≥ 5). (F) iWAT of mice. Bar, 1cm. (G) eWAT weight /
577 bodyweight, (n ≥ 5). (H) The liver of mice. (I) HE staining of mice liver sections. Bar,
578 100 μm. (J) Liver triglyceride (TG) levels. (K) The *Ampk*, *Cpt1*, *Acca*, *Atgl* mRNA
579 expression level in mice liver, (n ≥ 5). (L) SCAD activity in liver of mice, (n = 5). The
580 data are expressed as mean ± SD. *P < 0.05 **P < 0.01 .
581
582 Figure S1.
583 (A) Triglyceride content with OA/PA (n = 3). (B) BATF mRNA levels. NC, negative
584 control group; siBATF, BATF inhibition group, (n = 3). (C) Triglyceride content with
585 OA/PA treatment, (n = 5). (D) Triglyceride content with OA/PA when BATF was
586 overexpressed, (n = 3). The data are expressed as mean ± SD. *P < 0.05 **P < 0.01.
587
588 Figure S2.
589 (A) Fasting blood glucose level in mice, (n= 8-10). (B) Glucose tolerance test and (C)
590 quantitative analysis, (n = 5-6). The data are expressed as mean ± SD. *P < 0.05 **P
591 < 0.01.
592
593

Fig.1

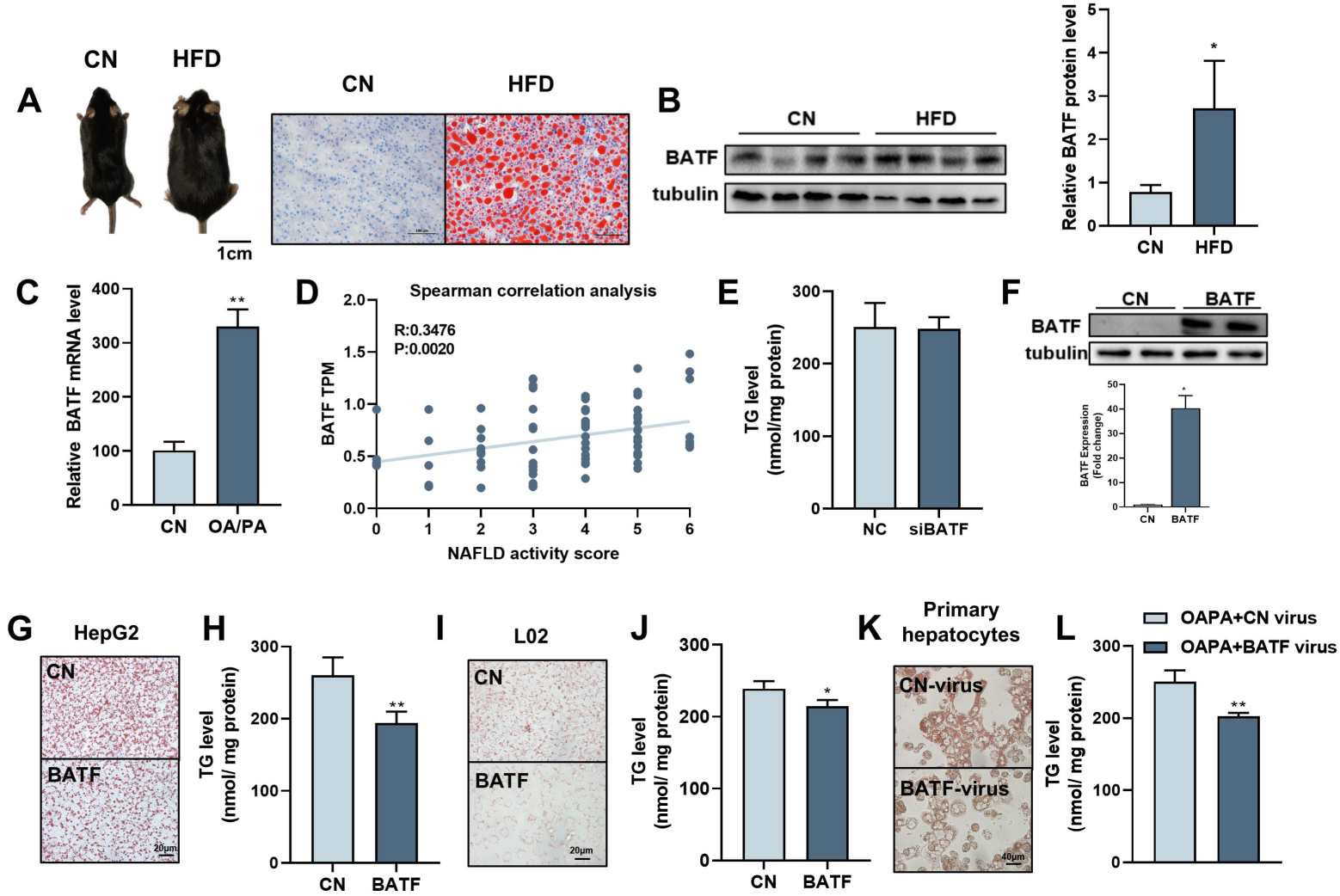
A
CN
HFD
1cm
CN
HFD
B
CN
HFD
BATF
tubulin
Relative BATF protein level
CN
HFD
C
Relative BATF mRNA level
CN
OA/PA
D
Spearman correlation analysis
R:0.3476
P:0.0020
BATF TPM
NAFLD activity score
E
TG level (nmol/mg protein)
NC
siBATF
F
CN
BATF
BATF
tubulin
BATF Expression (Fold change)
CN
BATF
G
HepG2
CN
BATF
H
TG level (nmol/ mg protein)
CN
BATF
I
L02
CN
BATF
J
TG level (nmol/ mg protein)
CN
BATF
K
Primary hepatocytes
CN-virus
BATF-virus
L
OAPA+CN virus
OAPA+BATF virus
TG level (nmol/ mg protein)

Fig.S1

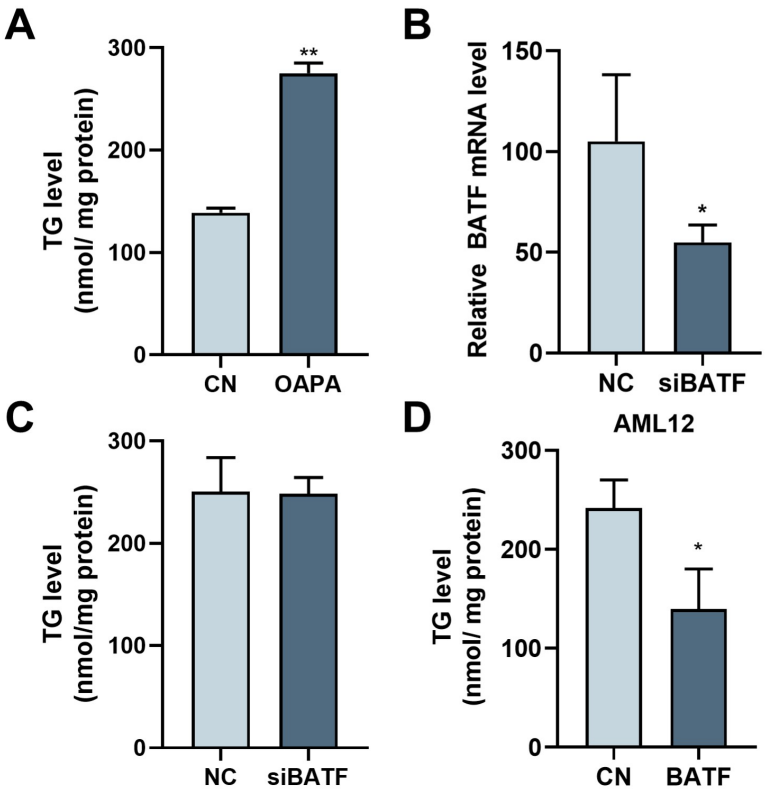
A
TG level
(nmol/ mg protein)
300
200
100
0
**
CN
OAPA
B
Relative BATF mRNA level
150
100
50
0
*
NC
siBATF
C
TG level
(nmol/mg protein)
300
200
100
0
NC
siBATF
D
AML12
TG level
(nmol/ mg protein)
300
200
100
0
*
CN
BATF

Fig.2

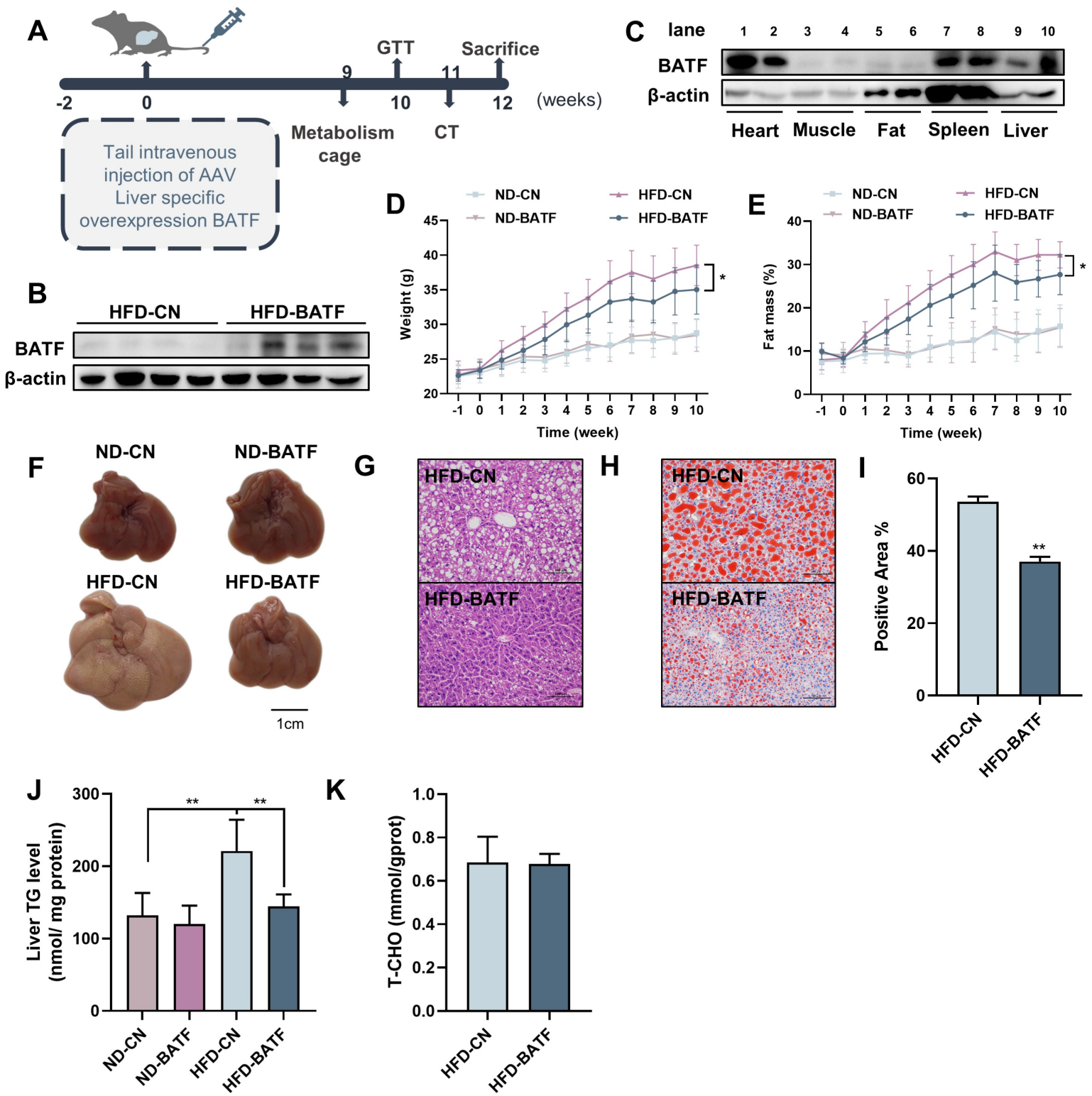
A
GTT
Sacrifice
-2
0
9
10
11
12
(weeks)
Metabolism cage
CT
Tail intravenous injection of AAV Liver specific overexpression BATF
B
HFD-CN
HFD-BATF
BATF
β-actin
C
lane
1 2 3 4 5 6 7 8 9 10
BATF
β-actin
Heart
Muscle
Fat
Spleen
Liver
D
ND-CN
ND-BATF
HFD-CN
HFD-BATF
Weight (g)
Time (week)
E
ND-CN
ND-BATF
HFD-CN
HFD-BATF
Fat mass (%)
Time (week)
F
ND-CN
ND-BATF
HFD-CN
HFD-BATF
1cm
G
HFD-CN
HFD-BATF
H
HFD-CN
HFD-BATF
I
Positive Area %
HFD-CN
HFD-BATF
J
Liver TG level (nmol/ mg protein)
ND-CN
ND-BATF
HFD-CN
HFD-BATF
K
T-CHO (mmol/gprot)
HFD-CN
HFD-BATF

Fig.S2

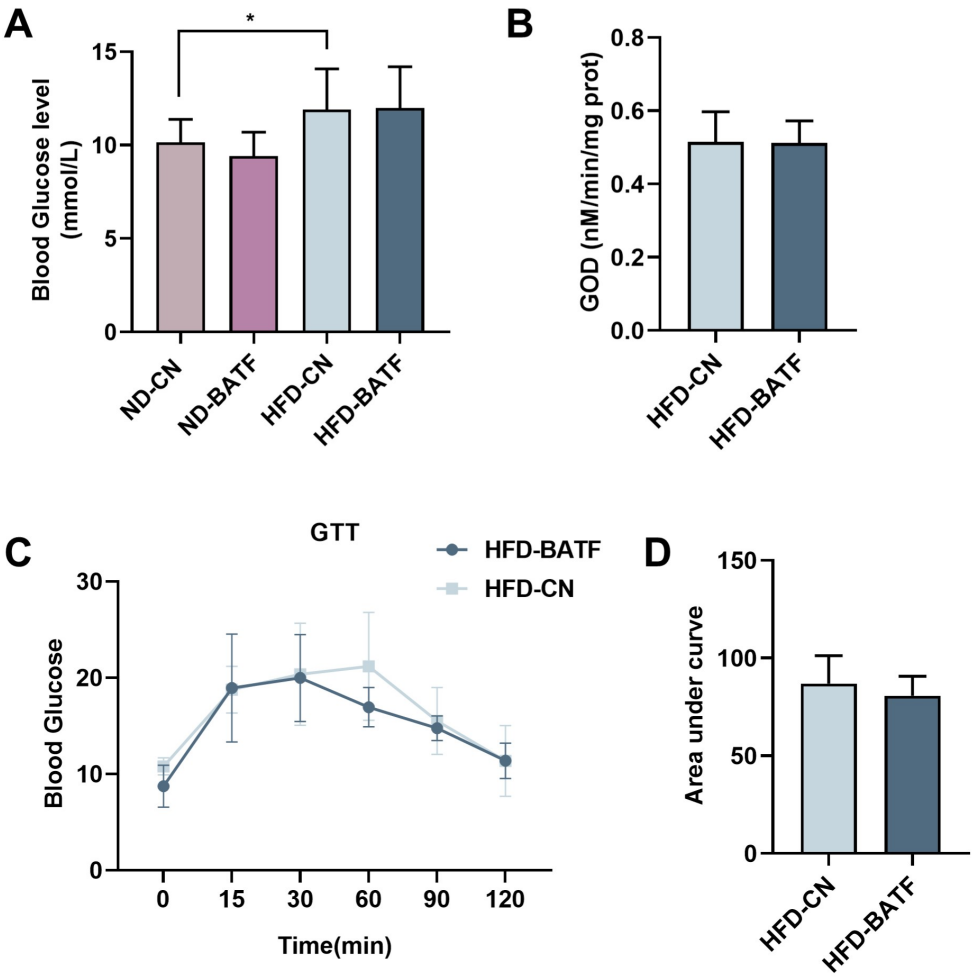
A
*
Blood Glucose level (mmol/L)
15
10
5
0
ND-CN
ND-BATF
HFD-CN
HFD-BATF
B
GOD (nM/min/mg prot)
0.8
0.6
0.4
0.2
0.0
HFD-CN
HFD-BATF
C
GTT
HFD-BATF
HFD-CN
Blood Glucose
30
20
10
0
0
15
30
60
90
120
Time(min)
D
Area under curve
150
100
50
0
HFD-CN
HFD-BATF

Fig.3

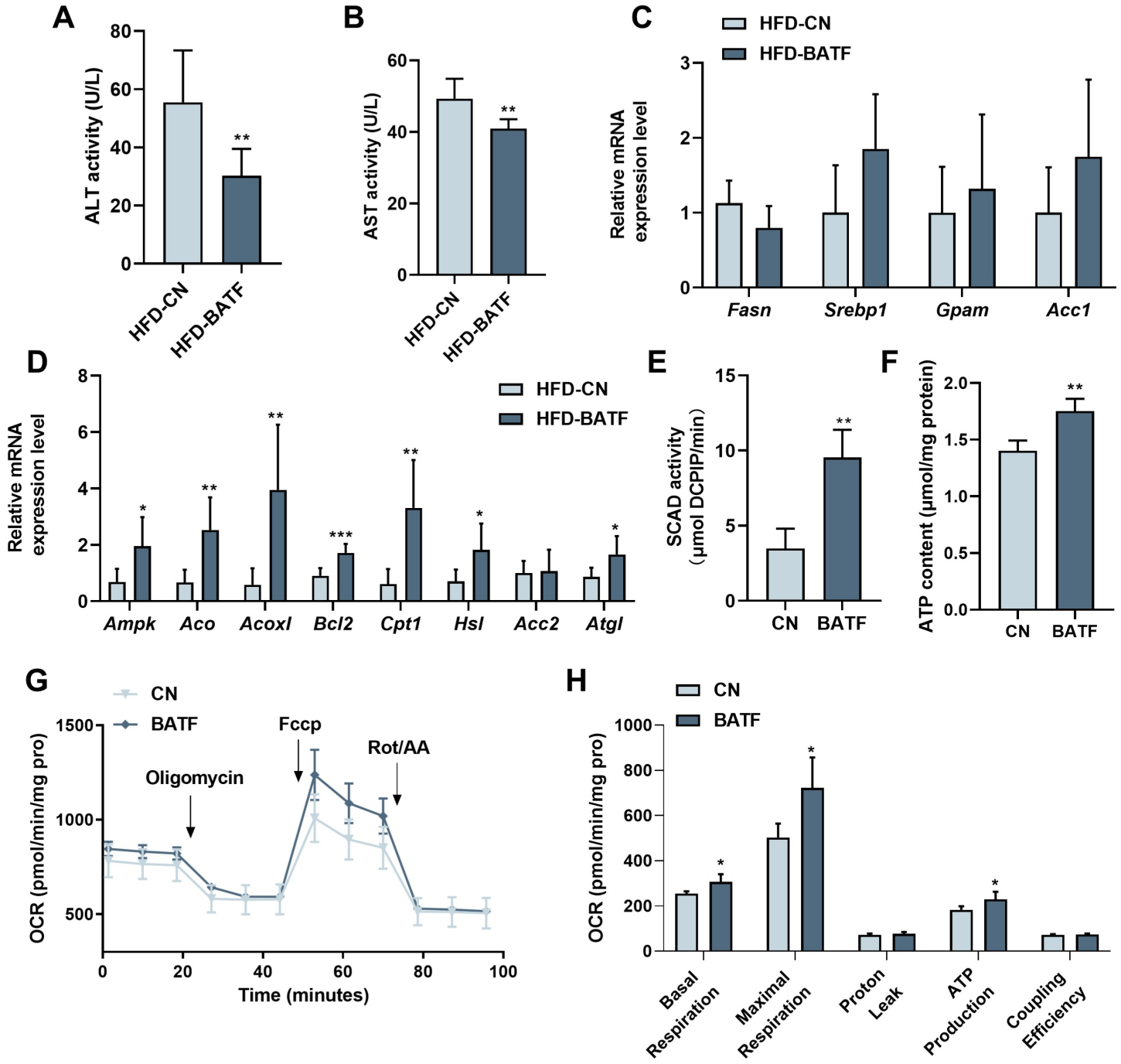
A
ALT activity (U/L)
80
60
40
20
0
**
HFD-CN
HFD-BATF
B
AST activity (U/L)
60
40
20
0
**
HFD-CN
HFD-BATF
C
HFD-CN
HFD-BATF
Relative mRNA expression level
3
2
1
0
Fasn
Srebp1
Gpam
Acc1
D
Relative mRNA expression level
8
6
4
2
0
HFD-CN
HFD-BATF
*
**
**
***
**
*
*
Ampk
Aco
Acoxl
Bcl2
Cpt1
Hsl
Acc2
Atgl
E
SCAD activity (μmol DCPIP/min)
15
10
5
0
**
CN
BATF
F
ATP content (μmol/mg protein)
2.0
1.5
1.0
0.5
0.0
**
CN
BATF
G
CN
BATF
OCR (pmol/min/mg pro)
1500
1000
500
Oligomycin
Fccp
Rot/AA
0
20
40
60
80
100
Time (minutes)
H
CN
BATF
OCR (pmol/min/mg pro)
1000
800
600
400
200
0
*
*
*
Basal Respiration
Maximal Respiration
Proton Leak
ATP Production
Coupling Efficiency

Fig.4

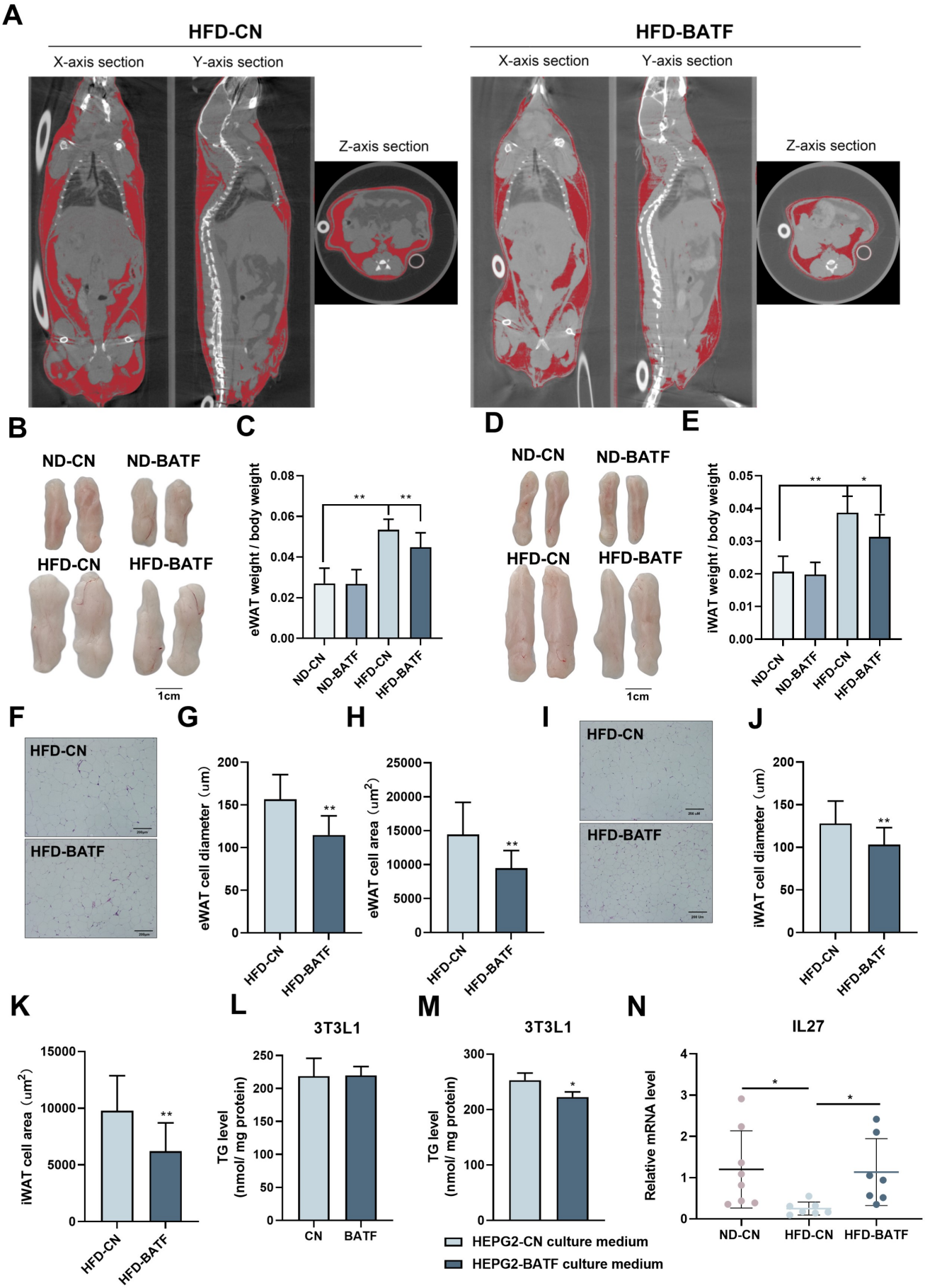
A
HFD-CN
X-axis section
Y-axis section
Z-axis section
HFD-BATF
X-axis section
Y-axis section
Z-axis section
B
ND-CN
ND-BATF
HFD-CN
HFD-BATF
1cm
C
eWAT weight / body weight
0.08
0.06
0.04
0.02
0.00
**
**
ND-CN
ND-BATF
HFD-CN
HFD-BATF
D
ND-CN
ND-BATF
HFD-CN
HFD-BATF
1cm
E
iWAT weight / body weight
0.05
0.04
0.03
0.02
0.01
0.00
**
*
ND-CN
ND-BATF
HFD-CN
HFD-BATF
F
HFD-CN
HFD-BATF
G
eWAT cell diameter（um）
200
150
100
50
0
**
HFD-CN
HFD-BATF
H
eWAT cell area（um2）
25000
20000
15000
10000
5000
0
**
HFD-CN
HFD-BATF
I
HFD-CN
HFD-BATF
J
iWAT cell diameter（um）
200
150
100
50
0
**
HFD-CN
HFD-BATF
K
iWAT cell area（um2）
15000
10000
5000
0
**
HFD-CN
HFD-BATF
L
3T3L1
TG level
(nmol/ mg protein)
250
200
150
100
50
0
CN
BATF
M
3T3L1
TG level
(nmol/ mg protein)
300
200
100
0
*
HEPG2-CN culture medium
HEPG2-BATF culture medium
N
IL27
Relative mRNA level
4
3
2
1
0
*
*
ND-CN
HFD-CN
HFD-BATF

Fig.5

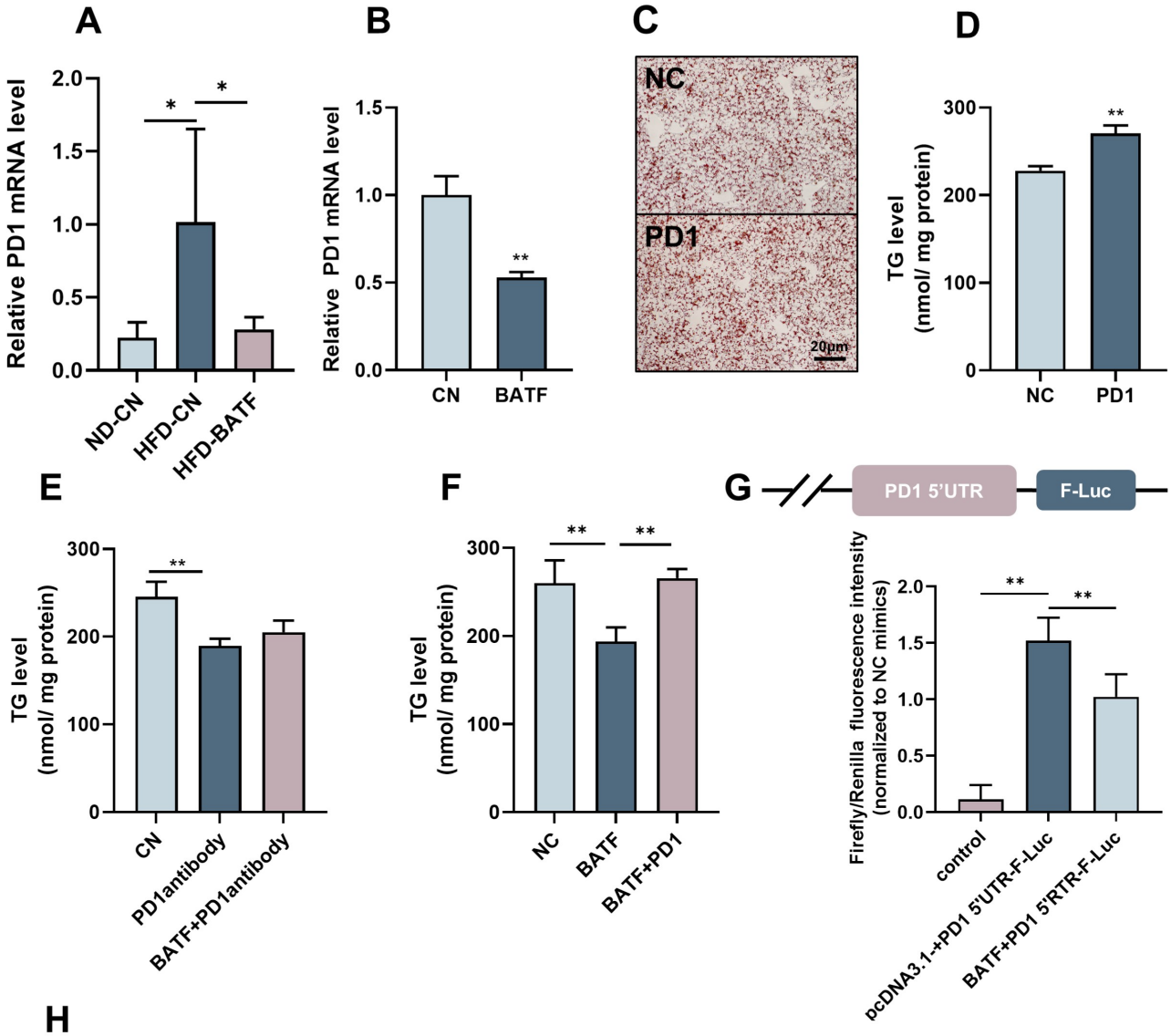
A
Relative PD1 mRNA level
2.0
1.5
1.0
0.5
0.0
*
*
ND-CN
HFD-CN
HFD-BATF
B
Relative PD1 mRNA level
1.5
1.0
0.5
0.0
**
CN
BATF
C
NC
PD1
20μm
D
TG level
(nmol/ mg protein)
300
200
100
0
**
NC
PD1
E
TG level
(nmol/ mg protein)
300
200
100
0
**
CN
PD1antibody
BATF+PD1antibody
F
TG level
(nmol/ mg protein)
300
200
100
0
**
**
NC
BATF
BATF+PD1
G
PD1 5'UTR
F-Luc
Firefly/Renilla fluorescence intensity
(normalized to NC mimics)
2.0
1.5
1.0
0.5
0.0
**
**
control
pcDNA3.1-+PD1 5'UTR-F-Luc
BATF+PD1 5'RTR-F-Luc

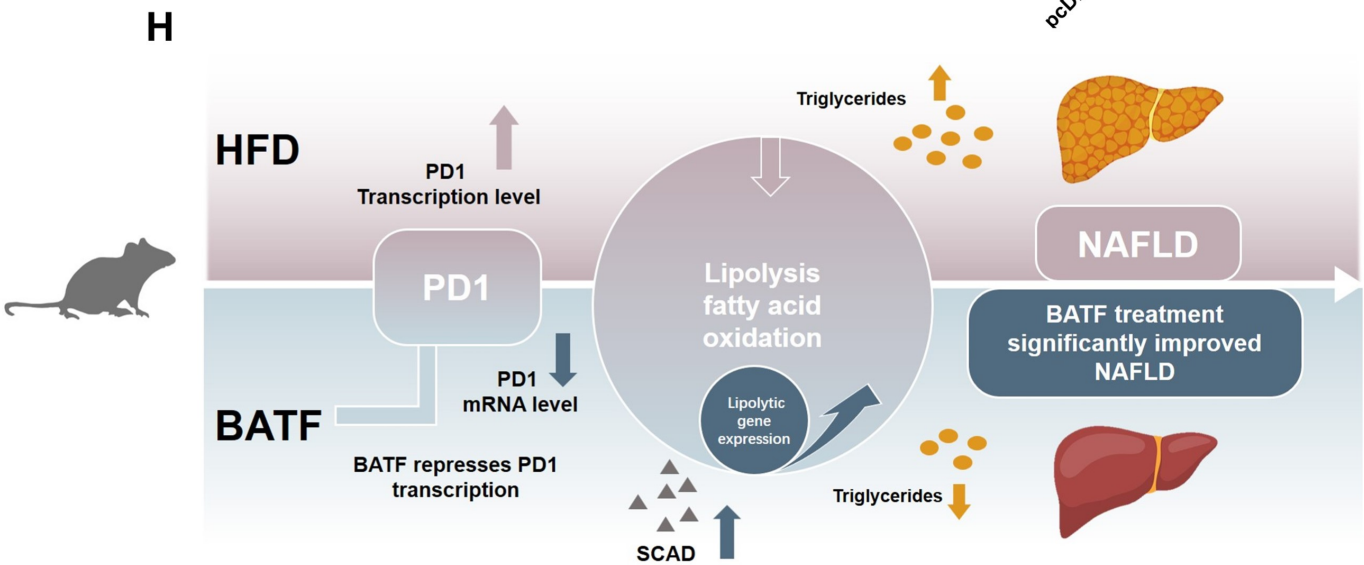
H
HFD
PD1
Transcription level
Triglycerides
NAFLD
PD1
Lipolysis
fatty acid
oxidation
BATF treatment
significantly improved
NAFLD
BATF
PD1
mRNA level
Lipolytic
gene
expression
BATF represses PD1
transcription
Triglycerides
SCAD

Fig.6

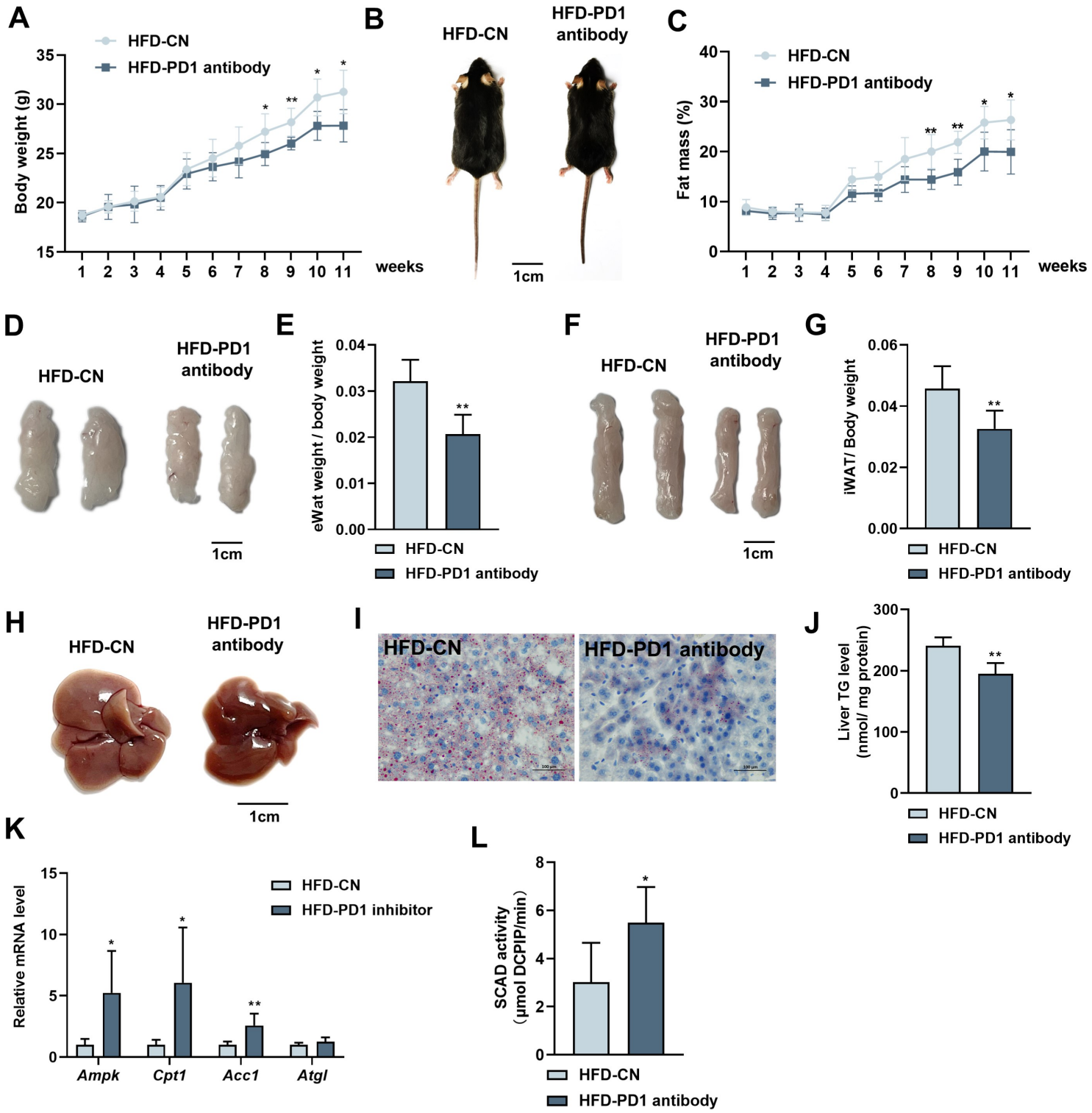
A
HFD-CN
HFD-PD1 antibody
Body weight (g)
weeks
B
HFD-CN
HFD-PD1 antibody
1cm
C
HFD-CN
HFD-PD1 antibody
Fat mass (%)
weeks
D
HFD-CN
HFD-PD1 antibody
1cm
E
eWat weight / body weight
HFD-CN
HFD-PD1 antibody
F
HFD-CN
HFD-PD1 antibody
1cm
G
iWAT/ Body weight
HFD-CN
HFD-PD1 antibody
H
HFD-CN
HFD-PD1 antibody
1cm
I
HFD-CN
HFD-PD1 antibody
J
Liver TG level (nmol/ mg protein)
HFD-CN
HFD-PD1 antibody
K
Relative mRNA level
HFD-CN
HFD-PD1 inhibitor
Ampk
Cpt1
Acc1
Atgl
L
SCAD activity (μmol DCPIP/min)
HFD-CN
HFD-PD1 antibody